Surface & Coatings Technology 264 (2015) 41–48

Contents lists available at ScienceDirect

Surface & Coatings Technology

journal homepage: www.elsevier.com/locate/surfcoat

A first-principles study of structure, elasticity and thermal decomposition of $Ti_{1-x}TM_xN$ alloys (TM = Y, Zr, Nb, Hf, and Ta)

Pengfei Ou [a,b], Jiong Wang [a,c,*], Shunli Shang [d], Li Chen [a], Yong Du [a], Zi-Kui Liu [d], Feng Zheng [b]

[a] State Key Lab of Powder Metallurgy, Central South University, Changsha, Hunan 410083, China
[b] School of Materials Science and Engineering, Central South University, Changsha, Hunan 41083, China
[c] School of Metallurgy and Environment, Central South University, Changsha, Hunan 410083, China
[d] Department of Materials Science and Engineering, The Pennsylvania State University, University Park, PA 16802, USA

ARTICLE INFO

Article history:
Received 4 December 2014
Accepted in revised form 10 January 2015
Available online 15 January 2015

Keywords:
Nitride coatings
First-principles calculations
Enthalpy of mixing
Elastic properties

ABSTRACT

A systematic investigation concerning the effects of transition metals (TM = Y, Zr, Nb, Hf, and Ta) on the structure, elasticity and thermal decomposition of the TiN-based nitride coatings with a cubic rock-salt structure has been performed in terms of first-principles calculations. Calculated lattice parameters of $Ti_{1-x}TM_xN$ as a function of alloying concentration show positive derivations from the linearized Vegard's law, agreeing well with experimental and theoretical results. Positive enthalpies of mixing of $Ti_{1-x}TM_xN$ (TM = Y, Zr, and Hf) indicate that the formation of these alloys is energetically unfavored with respect to the mixing of the cubic phases. The predicted consolute temperature of $Ti_{1-x}Zr_xN$ agrees reasonably well with previous theoretical findings. The miscibility gaps disappear in the case of alloying TiN with NbN and TaN. Predicted elastic stiffness constants C_{11}, C_{12}, and C_{44} together with the aggregate polycrystalline properties of $Ti_{1-x}TM_xN$ are determined by an efficient strain–stress method. The present results indicate that the above nitride alloys are mechanically stable and addition of Nb and Ta increases the ductility, with Ta possessing the largest effect.

1. Introduction

Transition metal nitride (TMN) thin films are nowadays widely used in various applicative fields of technological importance, such as protective hard coatings for cutting tools [1–3], diffusion barriers or metallization layers in integrated circuits [4–6], and growth templates for group III-nitride semiconductor devices [7,8]. Titanium nitride (TiN) is one of the coatings developed for metal cutting tool applications, and remains a mainstay of the coating business due to its bright gold in color, hardness, and adaptability for most wear applications [9,10].

Being one of several approaches to enhance the functional properties of these materials, the current research strategy is driven by the prospect of synthesizing new multi-component or multinary hard coatings, by alloying TiN with different metal or non-metal nitrides [11–23]. For example, alloying element Y has been reported to enhance the adhesion between coating and substrate as well as the service lifetime of TiN coatings [18,19]; incorporation of Zr into TiN coating results in an enhanced hardness compared with binary TiN and ZrN coatings because of a solid solution strengthening mechanism [23]. Nb increases the hardness [20,21]; Zr and Ta could change significantly film texture, microstructure, grain size, and surface morphology of coatings [22].

Apart from the experimental researches for the TiN-based coating systems, good examples of demonstrating the ability of first-principles calculations for guiding the experiments by predicting chemistry-related trends are reported for various $Ti_{0.75}X_{0.25}N$ ternary systems (e.g., Refs. [24,25]). In Ref. [24], X includes Cr, Zr, Nb, V, W, Mo and Al, and in Ref. [25] X covers all the transition metals. In Ref. [26] the alloying-related trend concerned with Ti-Al-X-N quaternary systems was reported. The structure and elastic properties of metastable ternary $Ti_{1-x}Zr_xN$ alloys were systematically investigated by Abadias et al. [27] using thin film growth and ab-initio calculations. The structural and elastic properties of $Ti_{1-x}Ta_xN$ alloys have been computed by means of first-principles calculations on disordered alloys with the VCA framework and ordered supercells [28]. Trends in formation energies and elastic moduli of ternary transition metal nitrides $M^1_{0.5}M^2_{0.5}N$ ($M^{1,2}$ = Ti, Zr, Hf, V, Nb or Ta) were systematically studied by Petrman et al. [29] by using the plane-wave self-consistent field.

In addition, the age-hardening of Ti–Zr–N coatings, due to the spinodal decomposition of c-$Ti_{1-x}Zr_xN$ into nano-size cubic Ti-rich and Zr-rich domains at elevated temperatures has attracted much attention. Phase relationships between binary nitrides TiN and ZrN reported by Duwez and Odell [30] indicate that these two compounds form a single-phase solid solution after heating at temperature greater than 2000 °C. Holleck et al. [31] also show a miscibility gap at

* Corresponding author at: State Key Lab of Powder Metallurgy, Central South University, Changsha, Hunan 410083, China. Tel.: +86 731 88877963; fax: +86 731 88710855.
E-mail addresses: wangjionga@csu.edu.cn, wangjionga@gmail.com (J. Wang).

http://dx.doi.org/10.1016/j.surfcoat.2015.01.024
0257-8972/

temperature less than 2000 °C between these two compounds. Hoerling et al. [32] investigated the properties of $Ti_{1-x}Zr_xN$ coating using cathodic arc evaporation deposition combined with first-principles calculations. It is concluded that single-phase c-$Ti_{1-x}Zr_xN$ is energetically favored with respect to a two-phase mixture of c-TiN and c-ZrN over a wide range of composition. Additionally, no phase transformation was observed during annealing of c-$Ti_{1-x}Zr_xN$ coating between 600 and 1200 °C. Wang et al. [33] predicted that the consolute temperature of c-$Ti_{1-x}Zr_xN$ reduces from 2670 to 1880 K if one accounts for the contribution of lattice vibrations of the free energy. On the contrary, the consolute temperatures of c-$Ti_{1-x}Zr_xN$ increase from 1900 to 1970 K with increasing pressure from 0 to 30 GPa.

In the present work, we use first-principles calculations to provide better understanding of the structure, phase stability and elastic properties of $Ti_{1-x}TM_xN$ (TM = Y, Zr, Nb, Hf and Ta) pseudo-binary alloys. We provide an overview of enthalpies of mixing and elastic moduli, namely bulk modulus (B), shear modulus (G) and Young's modulus (E). In addition, we evaluate the effect of increasing the valence electron concentration on the ductility of these alloys, to identify candidate materials for potentially hard coatings with enhanced ductility. The remainder of this paper is organized as follows. Section 2 briefly introduces the methodologies, including the details of the first-principles calculations, and an efficient strain–stress method to determine elastic stiffness constants. In Section 3, structure, thermal decomposition and elasticity of $Ti_{1-x}TM_xN$ alloys are presented and discussed, and the trends in terms of composition and temperature are rationalized. Section 4 summarizes the main conclusions in the present work.

2. Methodology

2.1. First-principles calculations

First-principles calculations in the present work are performed by means of the Vienna Ab-initio Simulation Package (VASP) [34,35] with the ion-electron interaction described by the projector augmented-wave (PAW) method [36], and the exchange–correlation functional depicted by the generalized gradient approximation (GGA) as parameterized by Perdew–Burke–Ernzerhof [37]. k-point meshes ($17 \times 17 \times 17$ in the case of 8-atom supercells and $6 \times 6 \times 6$ of 64-atom supercells) for Brillouin zone sampling using the Monkhorst–Pack scheme [34] together with 520 eV plane wave energy cutoff are employed based on our tests. The atomic positions and cell shape are fully relaxed until the residual forces acting on ions are smaller than 0.01 eV/Å, and the energy convergence criterion of the electronic self-consistency is at least 10^{-6} eV/atom for all calculations. Reciprocal-space energy integration is performed using the Methfessel–Paxton technique [38] for structure relaxations, while the tetrahedron method incorporating with Blöchl corrections [39] is adopted for the final calculations of total energies. The 8-atom supercells in the case of binary metal nitrides, and 64-atom supercells in the case of ternary alloys are used herein to model the cubic B1 rock-salt structure $Ti_{1-x}TM_xN$ alloys (Fig. 1, more details in Ref. [27]).

To assess the short-range order (SRO) in our alloys we use the Warren–Cowley α parameter as done in reference [40]. For pseudo-binaries $M1_{1-x}M2_xN$, this is defined as $\alpha = 1 - P_{M2}(d_n)/x$, where $P_{M2}(d_n)$ is the probability of finding an atom M2 on the n^{th} neighboring shell, at a interatomic distance d, from an M1 atom. Ideal solid solutions will thus have α values close to zero on all neighboring shells. Negative α values on any neighboring shell are indicative of ordering. This means that the probability of finding M1 atoms, on spheres of radii d_n centered on M2 atoms, is larger than average M1 concentration on the metallic sublattice. Positive α values, instead, are indicative of clustering, i.e. the probability of finding M1 atoms on neighboring shells centered on M1 atoms is larger than the average M1 concentrations on the metallic sublattice. Thus, both positive and negative α values, with extremes $+1$ and -1, are indicative of highly correlated atomic positions on neighboring spherical shells. Fig. 1 shows the atomic configurations together with the values of Warren–Cowley short-range order (SRO) for the 64-atom supercells studied herein, as calculated on neighboring spherical shell extending up to seven interatomic distances ($7 \times d_{NN} \sim 1.4$ nm).

2.2. Ground state properties

In order to estimate the ground state properties, nine energy versus volume data points calculated from first-principles were used to fit the four-parameter Birch–Murnaghan equation of state (EOS) [41–43], with the largest volume change of ±5% with respect to the equilibrium volume:

$$E(V) = a + bV^{-2/3} + cV^{-4/3} + dV^{-6/3} \quad (1)$$

where, a, b, c, and d are fitting parameters, and V is the volume. The structural properties, including equilibrium volume V_0, total energy E_0, bulk modulus B_0 and its pressure derivative B_0' can be calculated from this EOS.

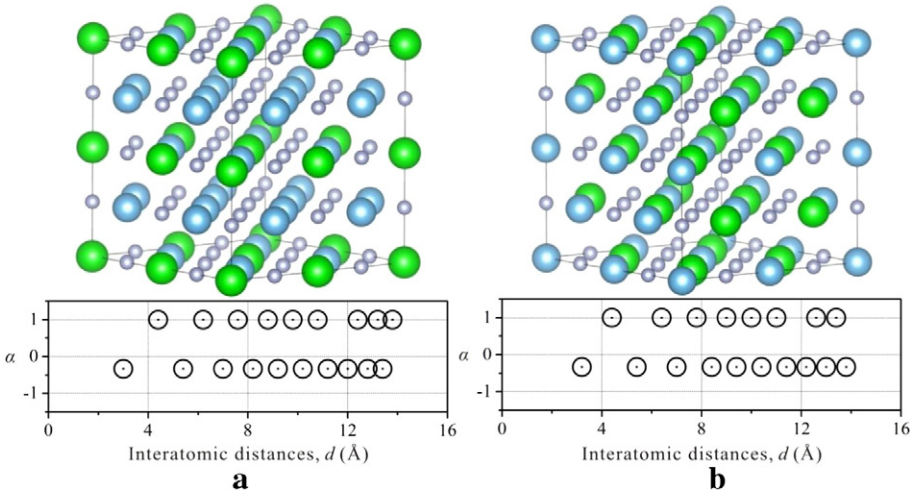

Fig. 1. Atomic arrangements on the metallic sublattice, together with Warren–Cowley short range order parameters, plotted as a function of interatomic distances, (a) $x = 0.25$ or 0.75, (b) $x = 0.5$ for the $Ti_{1-x}TM_xN$ alloys with TM = Y, Zr, Nb, Hf, and Ta.

2.3. Enthalpy of mixing

The enthalpy of mixing, ΔH_{mix}, is calculated as

$$\Delta H_{mix} = E(Ti_{1-x}TM_xN) - [(1-x)E(TiN) + xE(TMN)] \quad (2)$$

where $E(TMN)$ is the total energy of binary alloy TMN, and $E(Ti_{1-x}TM_xN)$ is the energy of the ternary alloy. Enthalpy of mixing indicates the energy gain (when positive) or loss (when negative) with respect to the end-members of binary nitrides, implying whether the alloy is stable ($\Delta H_{mix} < 0$) or unstable ($\Delta H_{mix} > 0$) with respect to the binary nitrides.

2.4. Elastic properties

An efficient strain–stress method demonstrated by Shang et al. [44,45] is employed to calculate the elastic stiffness constants. Under the frame of this methodology, a set of strains $\varepsilon = (\varepsilon_1, \varepsilon_2, \varepsilon_3, \varepsilon_4, \varepsilon_5, \varepsilon_6)$ (where $\varepsilon_1, \varepsilon_2$ and ε_3 are normal strains and the others are shear strains) is imposed on a crystal with lattice vectors R specified in Cartesian coordinates.

$$R = \begin{bmatrix} a_1 & a_2 & a_3 \\ b_1 & b_2 & b_3 \\ c_1 & c_2 & c_3 \end{bmatrix} \quad (3)$$

where a_1 is the first (or x) component of lattice vector $\vec{a}$, b_2 the second (or y component of lattice vector $\vec{b}$, and so on. As a result, the crystal vectors before (R) and after ($\overline{R}$) deformation can be described as follows:

$$\overline{R} = R\begin{bmatrix} 1+\varepsilon_1 & \varepsilon_6/2 & \varepsilon_5/2 \\ \varepsilon_6/2 & 1+\varepsilon_2 & \varepsilon_4/2 \\ \varepsilon_5/2 & \varepsilon_4/2 & 1+\varepsilon_3 \end{bmatrix} \quad (4)$$

In the present work, the following linearly independent sets of strains are applied:

$$\begin{bmatrix} s & 0 & 0 & 0 & 0 & 0 \\ 0 & s & 0 & 0 & 0 & 0 \\ 0 & 0 & s & 0 & 0 & 0 \\ 0 & 0 & 0 & s & 0 & 0 \\ 0 & 0 & 0 & 0 & s & 0 \\ 0 & 0 & 0 & 0 & 0 & s \end{bmatrix} \quad (5)$$

with s equals a certain value and each row being one set of strains. The corresponding changes of stresses ($\sigma = \sigma_1, \sigma_2, \sigma_3, \sigma_4, \sigma_5$, and σ_6) for the deformed crystals due to each set of applied strains will be determined through first-principles calculations. The elastic stiffness constants (C_{ij}'s) are then obtained from the n sets of strains (ε) and the corresponding changes of stresses (σ) based on the general Hook's law:

$$\begin{bmatrix} C_{11} & C_{12} & C_{13} & C_{14} & C_{15} & C_{16} \\ C_{21} & C_{22} & C_{23} & C_{24} & C_{25} & C_{26} \\ C_{31} & C_{32} & C_{33} & C_{34} & C_{35} & C_{36} \\ C_{41} & C_{42} & C_{43} & C_{44} & C_{45} & C_{46} \\ C_{51} & C_{52} & C_{53} & C_{54} & C_{55} & C_{56} \\ C_{61} & C_{62} & C_{63} & C_{64} & C_{65} & C_{66} \end{bmatrix} = \begin{bmatrix} \varepsilon_{1,1} & \cdots & \varepsilon_{1,n} \\ \varepsilon_{2,1} & \cdots & \varepsilon_{2,n} \\ \varepsilon_{3,1} & \cdots & \varepsilon_{3,n} \\ \varepsilon_{4,1} & \cdots & \varepsilon_{4,n} \\ \varepsilon_{5,1} & \cdots & \varepsilon_{5,n} \\ \varepsilon_{6,1} & \cdots & \varepsilon_{6,n} \end{bmatrix}^{-1} \begin{bmatrix} \sigma_{1,1} & \cdots & \sigma_{1,n} \\ \sigma_{2,1} & \cdots & \sigma_{2,n} \\ \sigma_{3,1} & \cdots & \sigma_{3,n} \\ \sigma_{4,1} & \cdots & \sigma_{4,n} \\ \sigma_{5,1} & \cdots & \sigma_{5,n} \\ \sigma_{6,1} & \cdots & \sigma_{6,n} \end{bmatrix} \quad (6)$$

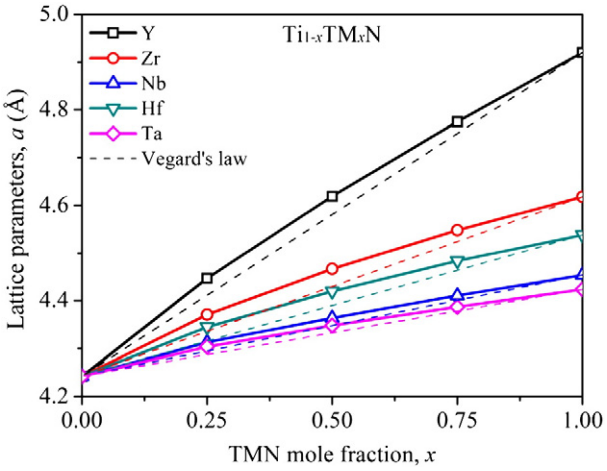

Fig. 2. Calculated lattice parameters, a (Å) as a function of composition x from Vegard's estimation for the $Ti_{1-x}TM_xN$ alloys with TM = Y, Zr, Nb, Hf and Ta.

where the superscript "-1" represents the pseudo-inverse, which can be solved based on the singular value decomposition method to get the least square solutions of elastic constants. Thus, the more strain uses, the more accurate the fitting results will be. It is also worth mentioning that, the minimum linearly independent sets of strains to determine the elastic constants are two for cubic, three for hexagonal and rhombohedral, four for tetragonal, and six for orthorhombic, monoclinic, and triclinic structures. Calculations are also performed for three different groups of strains with ± 0.007, ± 0.01 and ± 0.013, indicating that the present errors of C_{ij} are quite small (<1%). Thus, $s = \pm 0.01$ is chosen in the present work. Cubic systems exhibit three independent elastic stiffness constants, namely C_{11}, C_{12}, and C_{44}. Based on these elastic stiffness constants, the polycrystalline aggregate properties such as the bulk modulus B, shear modulus G, Young's modulus E, Zener's anisotropy A, and Poisson's ratio v can be computed via the Voigt–Reuss–Hill (VRH) approach [46].

$$B = B_V = B_R = \frac{1}{3}(C_{11} + 2C_{12}) \quad (7)$$

$$G_V = \frac{(C_{11} + C_{12} + 3C_{44})}{5} \quad (8)$$

$$G_R = \frac{5(C_{11} - C_{12})C_{44}}{4C_{44} + 3(C_{11} - C_{12})} \quad (9)$$

$$G = \frac{G_V + G_R}{2} \quad (10)$$

$$E = \frac{9BG}{3B + G} \quad (11)$$

$$A = \frac{2C_{44}}{C_{11} - C_{12}} \quad (12)$$

Table 1
Calculated lattice parameters a (Å), bulk modulus B_0 (GPa), and mixing enthalpies H_{mix} (meV/atom), of $Ti_{1-x}TM_xN$ systems for TM = Y, Zr, Nb, Hf, and Ta, as a function of TMN (x) mole fractions.

	$Ti_{1-x}Y_xN$			$Ti_{1-x}Zr_xN$			$Ti_{1-x}Nb_xN$			$Ti_{1-x}Hf_xN$			$Ti_{1-x}Ta_xN$		
x	a	B_0	H_{mix}	a	B_0	H_{mix}	a	B_0	H_{mix}	a	B_0	H_{mix}	a	B_0	H_{mix}
1.0	4.920	158	0	4.618	246	0	4.454	304	0	4.538	269	0	4.424	329	0
0.75	4.775	174	134	4.548	248	52	4.411	297	−28	4.484	267	12	4.387	317	−28
0.5	4.619	195	205	4.467	253	82	4.364	290	−60	4.420	266	24	4.348	304	−49
0.25	4.447	227	158	4.371	261	61	4.313	283	−36	4.345	269	16	4.304	290	−33
0.0	4.242	280	0	4.242	280	0	4.242	280	0	4.242	280	0	4.242	280	0

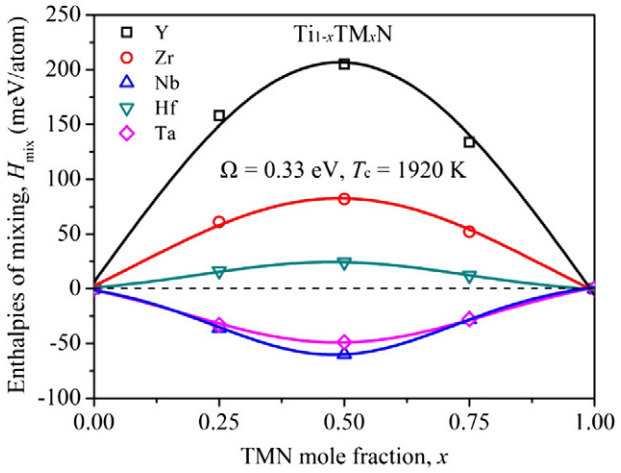

Fig. 3. Calculated enthalpies of mixing H_{mix} (meV/atom) and consolute temperature as a function of composition x for the $Ti_{1-x}TM_xN$ alloys with TM = Y, Zr, Nb, Hf, and Ta.

$$v = \frac{3B-2G}{2(3B+G)} \tag{13}$$

3. Results and discussion

3.1. Ground state properties and thermal decomposition

Fitting the energy-volume data points with Eq. (1) yields the structural properties of a, E_0, B and B_0'. Calculated lattice parameters of each $Ti_{1-x}TM_xN$ (TM = Y, Zr, Nb, Hf, and Ta) exhibit almost linear behaviors as a function of composition x. The linearly interpolated lattice parameter according to Vegard's law [47] reads

$$a_V(x) = (1-x)a_{TiN} + xa_{TMN} \tag{14}$$

First-principles calculated lattice parameters and bulk modulus are summarized in Table 1. Calculated lattice parameters and bulk modulus are in good agreement with available experimental results (Refs. [48–52]) and theoretical data (Refs. [24–26,29,53–55]). Predicted lattice parameters from GGA tend to underestimate the binding of crystals, resulting in larger lattice parameters compared with experimental values. However, the largest error regarding the predicted lattice parameter of TaN is less than 1%. Lattice parameters of $Ti_{1-x}TM_xN$ alloys from first-principles calculations are presented in Fig. 2. It can be seen that the lattice parameters of $Ti_{1-x}TM_xN$ (TM = Y, Zr, Nb, Hf, and Ta) alloys exhibit an almost linear behavior and increase with increasing the content of alloying elements. The difference $\Delta a = a - a_V$ for $Ti_{1-x}M_xN$ alloys as a function of composition shows that the linear Vegard's estimation is less accurate by a maximum of 0.69% for $x = 0.5$ in $Ti_{1-x}Y_xN$, which can be attributed to the larger lattice parameter of YN than TiN (a_{YN} = 4.89 Å, a_{TiN} = 4.24 Å). The $Ti_{0.5}TM_{0.5}N$ with TM = Zr, Hf, Nb, and Ta exhibits the differences Δa around 0.60%, 0.53%, 0.22% and 0.20%, respectively. These deviations should be considered when using Vegard's law as an estimate of lattice parameter.

Fig. 3 shows the enthalpies of mixing of $Ti_{1-x}TM_xN$ (TM = Y, Zr, Nb, Hf, and Ta) for the whole compositional range, $0 \le x \le 1$. The calculated results of mixing of enthalpies are summarized in Table 1. ΔH_{mix} is negative in the whole compositional range with addition of Nb or Ta into TiN system. This suggests that the $Ti_{1-x}Nb_xN$ and $Ti_{1-x}Ta_xN$ alloys are stable, a result previously shown in literature [14,26,56]. The driving force for decomposition is the largest for $Ti_{1-x}Y_xN$. The lattice difference between YN and TiN is about 16%, a value larger than what is "allowed" for substitutional solid solutions by Hume–Rothery rules. The positive enthalpies of mixing for $Ti_{1-x}Y_xN$, $Ti_{1-x}Zr_xN$ and $Ti_{1-x}Hf_xN$ indicate that the formation of these alloys are energetically unfavored with respect to the mixing of the cubic phases. $Ti_{1-x}Zr_xN$ has been shown to decompose spinodally before the stable cubic TiN and ZrN precipitate appear by experimental researches [30,31]. Therefore, ΔH_{mix} is positive for $Ti_{1-x}Zr_xN$, which is interpreted as the existence of miscibility gaps and spinodal decompositions. In order to estimate the consolute temperature T_c of miscibility gap, a simple model based on the mean field theory is employed [57], i.e.,

$$\Delta H_{mix} = \Omega x(1-x) \tag{15}$$

$$T_c = \frac{\Omega}{2k_B} \tag{16}$$

where T_c is defined as the upper temperature of immiscibility for a two-component liquid system, also known as upper consolute temperature

Table 2
Calculated elastic properties, including single crystal elastic stiffness constants C_{ij}'s (GPa), polycrystalline aggregate properties of bulk modulus B (GPa), shear modulus G (GPa), Young's modulus E (GPa), Zener's anisotropy A, Poisson's ratio v in VRH approach, Cauchy pressure C_{12}–C_{44} (GPa), and Pugh's index of ductility B/G, of $Ti_{1-x}TM_xN$ systems for TM = Y, Zr, Nb, Hf, and Ta, as a function of TMN (x) mole fractions.

	x	C_{11}	C_{12}	C_{44}	$C_{12}-C_{44}$	B	G	E	v	A	B/G
$Ti_{1-x}Y_xN$	1.0	318	78	123	−45	158	122	291	0.193	1.025	1.297
	0.75	357	85	128	−43	176	131	315	0.201	0.941	1.340
	0.5	406	94	134	−40	198	142	345	0.210	0.859	1.390
	0.25	479	108	146	−38	232	161	392	0.218	0.787	1.442
$Ti_{1-x}Zr_xN$	1.0	520	107	116	−9	245	146	366	0.251	0.562	1.671
	0.75	528	108	123	−15	248	153	380	0.245	0.586	1.625
	0.5	539	111	133	−22	254	161	399	0.238	0.621	1.575
	0.25	552	118	146	−28	263	171	422	0.232	0.673	1.534
$Ti_{1-x}Nb_xN$	1.0	641	136	75	61	304	125	330	0.319	0.297	2.431
	0.75	637	142	93	49	307	139	363	0.303	0.376	2.203
	0.5	635	127	112	15	296	157	399	0.275	0.441	1.893
	0.25	621	133	138	−5	296	174	436	0.254	0.566	1.702
$Ti_{1-x}Hf_xN$	1.0	589	110	119	−9	270	158	397	0.255	0.497	1.706
	0.75	580	111	130	−19	267	165	411	0.244	0.554	1.620
	0.5	577	114	139	−25	268	171	423	0.238	0.600	1.572
	0.25	585	120	149	−29	275	178	440	0.234	0.641	1.543
$Ti_{1-x}Ta_xN$	1.0	724	132	61	71	329	122	326	0.335	0.206	2.695
	0.75	684	134	89	45	317	143	372	0.304	0.324	2.224
	0.5	660	126	108	18	304	157	401	0.280	0.404	1.940
	0.25	623	129	133	−4	294	171	429	0.256	0.538	1.719
TiN	0.0	586	126	162	−36	279	186	458	0.227	0.704	1.498

or upper critical solution temperature, Ω is a fitting parameter, x is the mole fraction, and k_B is Boltzmann's constant. As is well known, a typical miscibility gap develops when Ω is positive. When Ω is positive and constant, the critical point of the miscibility gap occurs at 50 at.% of solute and at a temperature T_c [57]. For the $Ti_{1-x}Zr_xN$ alloys (see Fig. 3), the presently predicted consolute temperature of 1920 K without considering vibrational effect is lower than that of 2670 K without vibration estimated by Wang et al., [33] and one (~5000 K) by Hoerling et al. [32]. This discrepancy is mainly traceable from the treatment of disordered phases. The supercell method (64-atom supercell) is used herein, whereas the 32-atom special quasi-random structure (SQS) method was employed by Wang et al. [33] and an ideal solution was used by Hoerling et al. [32]. Regarding the random distribution of different atoms, the special quasirandom structure (SQS) is widely adopted in the first-principles community. An SQS represents a fully random alloy by means of a special configuration with a few (4–32) atoms to mimic the most relevant pair and multisite correlation functions of the solution and can be considered as a mixture of various microstates with its energy in the middle of the energy landscape of all microstates [58,59]. Therefore, the predicted consolute temperature from the SQS method by Wang et al. [33] is different from the present one. Regarding Hoerling's work [32], the total energies were calculated using a full-potential linear muffin tin orbital (FP-LMTO) method within the local density approximation of density functional theory. In terms of experiment [31], a miscibility gap with a consolute temperature below 2000 °C was estimated, which is consistent with our predication.

3.2. Single-crystal elastic stiffness constants

For a cubic crystal, its mechanical stability at a given pressure can be judged by Born stability criteria [60]:

$$C_{44}>0 \tag{17a}$$

$$C_{11}-|C_{12}|>0 \tag{17b}$$

$$C_{11}+2C_{12}>0 \tag{17c}$$

The calculated results of C_{ij}'s are summarized in Table 2 and plotted in Fig. 4, which are in a good agreement with the experimental results (Ref. [61]) and theoretically-predicted values (Refs. [29,51,54,62,63]) available in the literature. Elastic stiffness constant C_{11} of $Ti_{1-x}TM_xN$ is significantly stiffer than the other two elastic stiffness constants. It is found that C_{11}, C_{12} and C_{44} of $Ti_{1-x}TM_xN$ decrease with increasing the mole fraction of TMN (TM = Y, Zr, and Hf). Elastic stiffness constants of YN, ZrN and HfN show a trend of $C_{11} > C_{44} > C_{12}$ while the relation of $C_{11} > C_{12} > C_{44}$ is shown for NbN and TaN. These trends are in accordance with the neutron scatting measurements [61]. TaN exhibits a large value of C_{11} and a small value of C_{44}, implying a low G and E despite diving a relatively large B compared to other nitrides. According to Eqs. (17a)–(17c) and Table 2, all the cubic rock-salt nitrides of $Ti_{1-x}TM_xN$ alloys are mechanically stable.

3.3. Polycrystalline aggregates elastic properties

Based on elastic stiffness constants, the aggregate polycrystalline bulk modulus, shear modulus and Young's modulus can be calculated from the Voigt–Reuss–Hill approximations [46]. The general trends of bulk modulus, shear modulus and Young's modulus are shown in Fig. 5 (see Table 2). It can be observed that the bulk moduli decrease with the increment of alloying elements, except for $Ti_{1-x}Nb_xN$ and $Ti_{1-x}Ta_xN$, demonstrating a drastic upward curve (Fig. 5a). Calculated bulk moduli from C_{ij}'s at zero pressure are in good agreement with those obtained by the EOS fitting, as shown in Table 1, indicating that the approach of the present work is reliable. For shear modulus (Fig. 5b) and

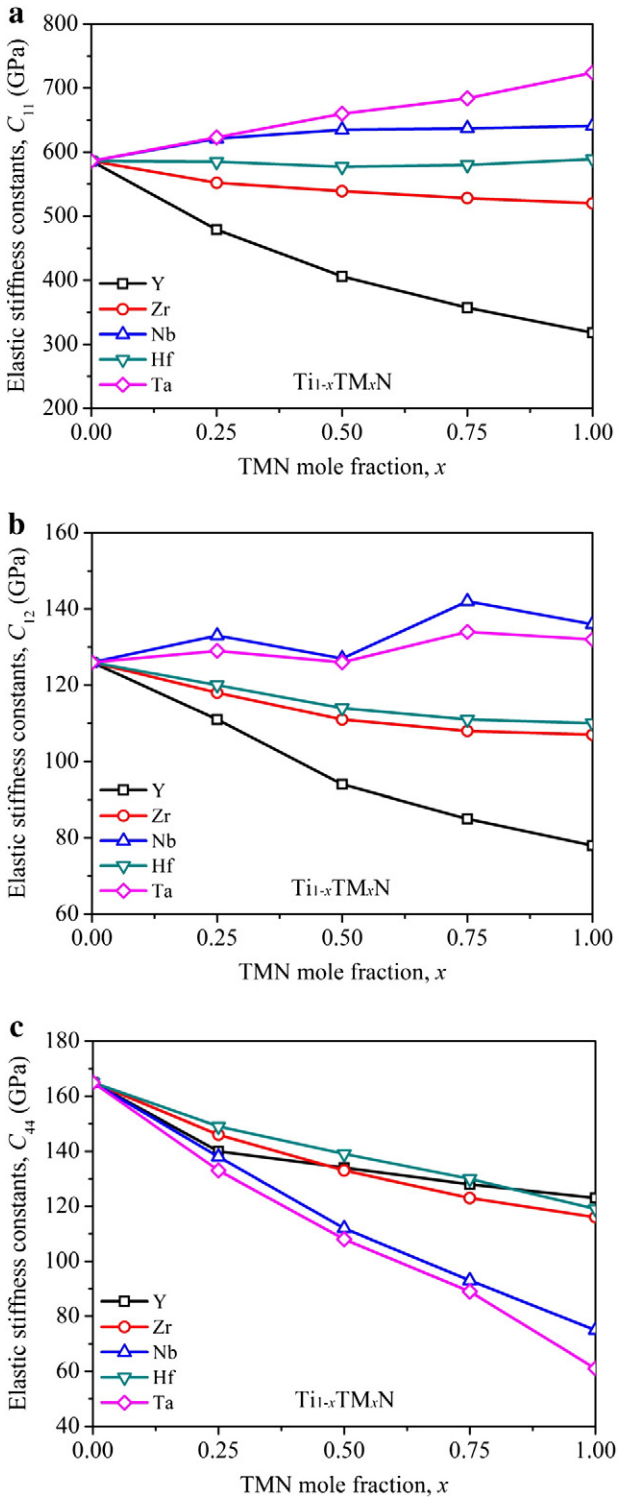

Fig. 4. Calculated elastic stiffness constants (a) C_{11}, (b) C_{12}, and (c) C_{44} as a function of composition x for the $Ti_{1-x}TM_xN$ alloys with TM = Y, Zr, Nb, Hf, and Ta.

Young's modulus (Fig. 5c), similar behaviors are observed for $Ti_{1-x}TM_xN$ alloys whose quantities decrease with an increase in TM content.

Cauchy pressure (C_{12}–C_{44}), Pugh's index of ductility (B/G), and Poisson's ratio (v) can be used to estimate the ductile or brittle nature for a given compound. The Cauchy pressure, defined as C_{12}–C_{44} for a cubic crystal, is considered to serve as an indication of ductility. If the pressure is positive (negative), the material is expected to be ductile (brittle) [64]. According to this criterion, TMN, $Ti_{0.25}TM_{0.75}N$, and $Ti_{0.5}TM_{0.5}N$ (TM = Nb, Ta) can be regarded as ductile materials, since

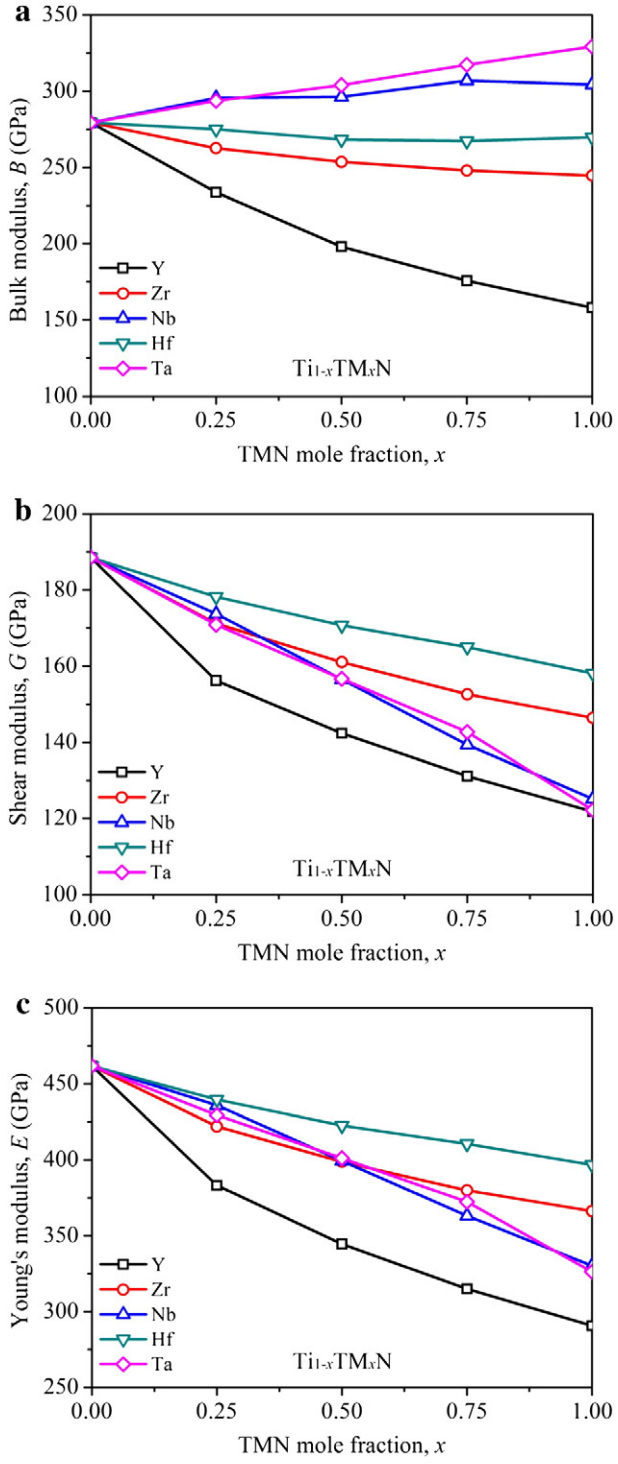

Fig. 5. Calculated (a) bulk modulus, B (GPa), (b) shear modulus, G (GPa) and (c) Young's modulus, E (GPa) as a function of composition x for the $Ti_{1-x}TM_xN$ alloys with TM = Y, Zr, Nb, Hf, and Ta.

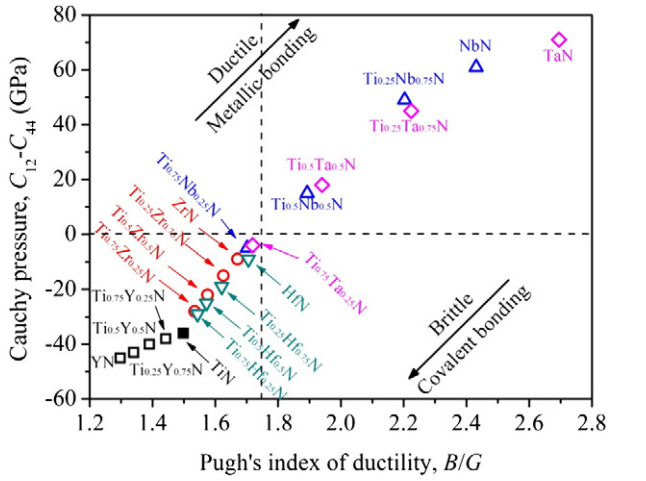

Fig. 6. Correlation between the Cauchy pressure, C_{12}–C_{44} (GPa) and Pugh's index of ductility, B/G, as a function of composition x for the $Ti_{1-x}TM_xN$ alloys with TM = Y, Zr, Nb, Hf, and Ta.

their Cauchy pressures are positive. On the contrary, other nitrides of $Ti_{1-x}TM_xN$ are considered to be brittle materials. Additionally, it has been suggested that the Cauchy pressure can be used to characterize the bonding type. As shown in Fig. 6, the perpendicular dashed line represents for Pugh's ratio $B/G = 1.75$ which is the separation of ductility and brittleness, and the horizontal dashed line for Cauchy pressure = 0, it is the boundary of positive and negative Cauchy pressure. Guided by the arrows in Fig. 6, the closer to the upper right corner, the more ductile and stronger metallic bonding; conversely, the closer to the lower left corner, the more brittle and the stronger covalent bonding. As shown in Fig. 6, the brittle TiN, YN, and ZrN are located in the lower left corner in the relationship of Cauchy pressure against B/G ratio, while NbN and TaN lie in the upper right corner. In contrast, HfN is almost close to the perpendicular dashed line of the critical value of B/G ratio proposed by Pugh [65] and exactly corresponds to the critical zero value of C_{12}–C_{44} defined by Pettifor [64]. The Cauchy pressures for $Ti_{1-x}TM_xN$ (TM = Nb, and Ta, with $x = 0.75$ and 0.5) are close to zero or positive, indicating that the predominant bonding behavior is metallic. Surprisingly, $Ti_{0.75}Nb_{0.25}N$ and $Ti_{0.75}Ta_{0.25}N$ are evidently moved to the lower left corner, resulting in a brittle behavior, while the other alloys including Nb and Ta are located in the upper right corner. Moreover, $Ti_{1-x}Y_xN$ is located in the lower left corner between the pure TiN and YN, indicating an increased brittleness with adding Y in TiN. The decrease of Cauchy pressure with increasing ZrN, NbN, HfN and TaN content (expect for YN) indicates a tendency towards stronger directional character of the bonds, which results in an increased resistance against shearing, a result reflected by the increasing trend of C_{44}. The trend in ductility criteria is clearly illustrated in Fig. 7 against with valence electron concentration (VEC), which is calculated as an average value of valence electrons per formula unit. Ti ([Ar] $3d^24s^2$), Y ([Kr] $4d^15s^2$), and N ([He] $2s^22p^3$) have 4, 3, and 5 valence electrons, respectively; hence VEC of $Ti_{0.5}Y_{0.5}N$ is $\frac{1}{2}\left(\frac{1}{2}(4+3)+5\right) = 8.5$. As demonstrated by both ab-initio calculations and experiments, $V_{0.5}W_{0.5}N$ and $V_{0.5}Mo_{0.5}N$ alloys (both have VEC = 10.5) can be synthesized as cubic single crystals, and are both hard and considerably more ductile compared to VN binaries [66–68], as beyond this value further filling of the d-t_{2g} metallic states might lead to instability of cubic phase [69]. In the alloys proposed herein, the metallic elements are selected to span the valence electron concentration (VEC) per unit formula from a minimum of 8 (in YN) up to a maximum of 10 (in TaN and NbN). Therein we also include as a reference point the results for TiN, compound with a VEC of 9 electrons per unit cell. The VEC dependence, consisting in increasing B/G ratios (Fig. 7a) and increasingly positive values for Cauchy pressures C_{12}–C_{44} (Fig. 7b), is obvious for all ternary nitrides considered in this study. The ductility monotonously increases with increasing number of VEC thus with an increasing amount of metallic bonding which agrees with previously theoretical calculations [29,56,70].

Generally, Poisson's ratio is connected with volume change in a material during uniaxial deformation and the nature of interatomic forces [71]. If $\nu = 0.5$, no volume change occurs, whereas $\nu < 0.5$ indicates that the volume change is associated with elastic deformation [72]. In the present work, calculated values of ν vary from 0.193 to 0.335,

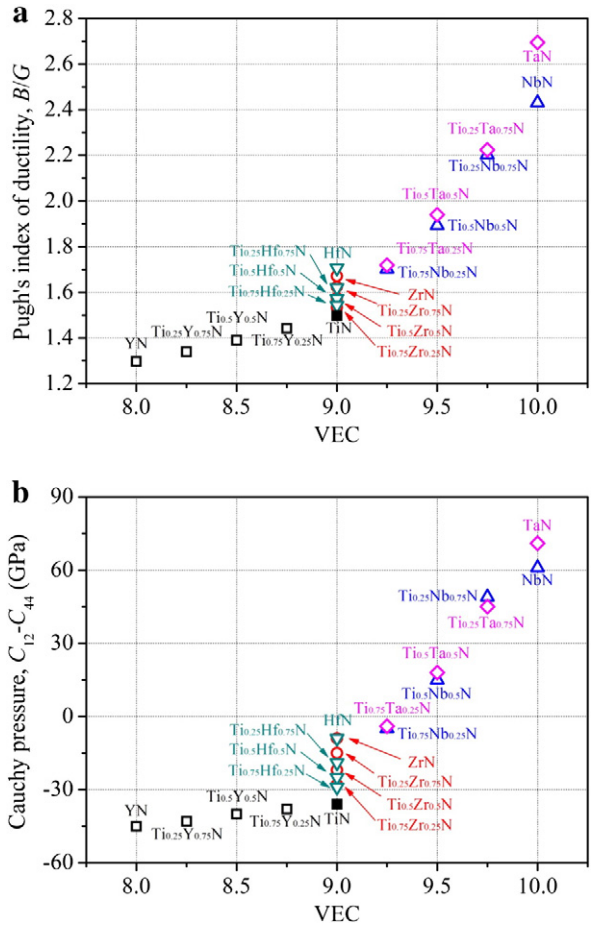

Fig. 7. VEC-induced trends in TiN-based transition metal nitrides. (a) *B*/*G* ratio dependence on VEC; (b) VEC effect on Cauchy pressure.

which means these $Ti_{1-x}TM_xN$ alloys are linked to a considerable volume change when deformation occurs.

Poisson's ratio *v* is also widely used to reflect the stability of a crystal against shear, which usually ranges from −1 to 0.5. The bigger Poisson's ratio is, the better the plasticity is. Moreover, the ductility or brittleness behavior can be characterized using Poisson's ratio *v* according to Frantsevich et al. [73], i.e., $v < 0.26$ for brittle materials and $v > 0.26$ for ductile materials. According to the calculated *B*/*G* ratios and *v* values shown in Table 2, all the binary and ternary nitrides can be regarded as brittle materials except for $Ti_{1-x}TM_xN$ (TM = Nb, Ta) with $x = 1$, 0.75, 0.5, because their *v* values are 0.319 (NbN), 0.335 (TaN), 0.303 ($Ti_{0.25}Nb_{0.75}N$), 0.304 ($Ti_{0.25}Ta_{0.75}N$), 0.275 ($Ti_{0.5}Nb_{0.5}N$) and 0.280 ($Ti_{0.5}Ta_{0.5}N$) respectively, which agree well with the former theoretical results [63]. Hence, the *B*/*G* ratios and Poisson's ratio *v* are in good agreement with the Cauchy pressure criterion, which confirms the classification of brittleness and ductility nature for $Ti_{1-x}TM_xN$ nitrides.

Microcracks are induced owing to the anisotropy of thermal expansion coefficient as well as the elastic anisotropy. It is thus important to calculate elastic anisotropy with a desire to tailor their durability [72]. The values of *A* in Table 2 depict the locally isotropy nature of YN ($A = 1.03$, similar to the well-known case of bcc W), as well as the anisotropy nature of NbN ($A = 0.297$) and TaN ($A = 0.207$). Additionally, Zener's elastic anisotropy accounts for the degree of dielectric breakdown and the resistance of mircocracks [74]. It is found that Zener's elastic anisotropy decreases with increasing mole fraction of TM in $Ti_{1-x}TM_xN$ except for $Ti_{1-x}Y_xN$. Therefore YN exhibits the highest degree of dielectric breakdown and the lowest resistance of mircocracks, due to the largest Zener's elastic anisotropy for YN ($A = 1.03$).

4. Conclusions

First-principles calculations have been employed to study the influence of alloying effects on the structure, elasticity and thermal decomposition of $Ti_{1-x}TM_xN$ (TM = Y, Zr, Nb, Hf, and Ta) coating alloys systematically. The obtained lattice parameters are in a good agreement with experimental results and other theoretical data. Analysis of the enthalpy of mixing suggests that alloying TiN with YN, ZrN, and HfN leads to a positive enthalpy of mixing which implies that the formation of these alloys is energetically unfavored with respect to the mixing of the cubic phases. On the other hand, Nb and Ta lead to a negative enthalpy of mixing, indicating that $Ti_{1-x}Nb_xN$ and $Ti_{1-x}Ta_xN$ are stable in comparison with the binary nitrides. Additionally, single crystal elastic stiffness constants together with the polycrystalline aggregate elastic properties including bulk modulus, shear modulus, Young's modulus, Poisson's ratio and anisotropy ratio, are also predicted and discussed. The present work shows the impact of alloying elements on the polycrystalline moduli and the intrinsic ductility parameter *B*/*G*. Addition of Ta and Nb evidently improves the bulk moduli and ductility of TiN, while ductility decreases as Y content is increased in TiN, which shows that Ta and Nb are the most promising strengtheners, closely followed by Zr and Hf. This phenomenon is shown to be primarily an effect of increased VEC per unit cell, and the revealed trend might be interesting and useful in designing new multi-component coatings.

Acknowledgments

This work was supported by the Postdoctoral Science Foundation of China (Grant No. 2014M552150), the National Science and Technology Major Project (2015ZX04005008) and the National Natural Science Foundation of China (Grant Nos., 51371201 and 51429101). Jiong Wang also greatly acknowledges the Postdoctoral Science Foundation of Central South University (Gant No. [2013]126650).

References

[1] O. Knotek, F. Löffler, G. Krämer, Surf. Coat. Technol. 54–55 (Part 1) (1992) 241–248.
[2] J. Lin, J.J. Moore, B. Mishra, M. Pinkas, W.D. Sproul, Acta Mater. 58 (2010) 1554–1564.
[3] U. Wiklund, S. Rubino, K. Kádas, N.V. Skorodumova, O. Eriksson, S. Hedberg, M. Collin, A. Olsson, K. Leifer, Acta Mater. 59 (2011) 68–74.
[4] J.-S. Chun, I. Petrov, J.E. Greene, J. Appl. Phys. 86 (1999) 3633–3641.
[5] A.E. Kaloyeros, E. Eisenbraun, Annu. Rev. Mater. Sci. 30 (2000) 363–385.
[6] M. Takeyama, A. Noya, T. Sase, A. Ohta, K. Sasaki, J. Vac. Sci. Technol. B 14 (1996) 674–678.
[7] G.M. Matenoglou, C.E. Lekka, L.E. Koutsokeras, G. Karras, C. Kosmidis, G.A. Evangelakis, P. Patsalas, J. Appl. Phys. 105 (2009) 103714.
[8] M.B. Takeyama, A. Noya, K. Sakanishi, J. Vac. Sci. Technol. B 18 (2000) 1333–1337.
[9] R. Buhl, H.K. Pulker, E. Moll, Thin Solid Films 80 (1981) 265–270.
[10] R.G. Gordon, MRS Bull. 25 (2000) 52–57.
[11] A.A. Andreev, V.M. Beresnev, M.A. Volosova, S.N. Grigor'ev, D.A. Kolesnikov, A.D. Pogrebnyak, I.V. Serdyuk, O.V. Sobol, P.V. Turbin, J. Frict. Wear 34 (2013) 175–182.
[12] S.M. Aouadi, J. Appl. Phys. 99 (2006) 053507.
[13] L.E. Koutsokeras, G. Abadias, C.E. Lekka, G.M. Matenoglou, D.F. Anagnostopoulos, G.A. Evangelakis, P. Patsalas, Appl. Phys. Lett. 93 (2008) 011904.
[14] G.M. Matenoglou, L.E. Koutsokeras, C.E. Lekka, G. Abadias, C. Kosmidis, G.A. Evangelakis, P. Patsalas, Surf. Coat. Technol. 204 (2009) 911–914.
[15] P.H. Mayrhofer, D. Music, T. Reeswinkel, H.G. Fuß, J.M. Schneider, Acta Mater. 56 (2008) 2469–2475.
[16] J. Neidhardt, Z. Czigány, B. Sartory, R. Tessadri, M. O'Sullivan, C. Mitterer, Acta Mater. 54 (2006) 4193–4200.
[17] F. Rovere, D. Music, J.M. Schneider, P.H. Mayrhofer, Acta Mater. 58 (2010) 2708–2715.
[18] Z.W. Zheng, Z.M. Yu, Surf. Coat. Technol. 204 (2010) 4107–4113.
[19] Z.M. Yu, Y.S. Niu, in: Z.Y. Jiang, S.Q. Li, J.M. Zeng, X.P. Liao, D.G. Yang (Eds.), Manufacturing Process Technology, Pts 1–5, Trans Tech Publications Ltd, Stafa-Zurich, 2011, pp. 747–751.
[20] B. Wollein, V. Buscaglia, W. Lengauer, M. Bohn, R. Musenich, P. Ettmayer, Surf. Interface Anal. 30 (2000) 368–371.
[21] V.N. Zhitomirsky, Surf. Coat. Technol. 201 (2007) 6122–6130.
[22] G. Abadias, L.E. Koutsokeras, S.N. Dub, G.N. Tolmachova, A. Debelle, T. Sauvage, P. Villechaise, J. Vac. Sci. Technol. A 28 (2010) 541–551.
[23] O. Knotek, F. Löffler, G. Krämer, Surf. Coat. Technol. 49 (1991) 325–329.
[24] K.Y. Chen, L.R. Zhao, J. Rodgers, J.S. Tse, J. Phys. D Appl. Phys. 36 (2003) 2725–2729.
[25] S. Huang, R.Z. Li, S.T. Qi, B. Chen, J. Shen, Int. J. Mod. Phys. B 28 (2014).

[26] D. Holec, L. Zhou, R. Rachbauer, P.H. Mayrhofer, J. Appl. Phys. 113 (2013) 113510.
[27] G. Abadias, V.I. Ivashchenko, L. Belliard, P. Djemia, Acta Mater. 60 (2012) 5601–5614.
[28] P. Djemia, M. Benhamida, K. Bouamama, L. Belliard, D. Faurie, G. Abadias, Surf. Coat. Technol. 215 (2013) 199–208.
[29] V. Petrman, J. Houska, J. Mater. Sci. 48 (2013) 7642–7651.
[30] P. Duwez, F. Odell, J. Electrochem. Soc. 97 (1950) 299–304.
[31] H. Holleck, J. Vac. Sci. Technol. A 4 (1986) 2661–2669.
[32] A. Hoerling, J. Sjölén, H. Willmann, T. Larsson, M. Odén, L. Hultman, Thin Solid Films 516 (2008) 6421–6431.
[33] A. Wang, S.-L. Shang, Y. Du, L. Chen, J. Wang, Z.-K. Liu, J. Mater. Sci. 47 (2012) 7621–7627.
[34] G. Kresse, J. Furthmüller, Phys. Rev. B 54 (1996) 11169–11186.
[35] G. Kresse, J. Hafner, Phys. Rev. B 49 (1994) 14251–14269.
[36] G. Kresse, D. Joubert, Phys. Rev. B 59 (1999) 1758–1775.
[37] J.P. Perdew, K. Burke, M. Ernzerhof, Phys. Rev. Lett. 77 (1996) 3865–3868.
[38] M. Methfessel, A.T. Paxton, Phys. Rev. B 40 (1989) 3616–3621.
[39] P.E. Blöchl, O. Jepsen, O.K. Andersen, Phys. Rev. B 49 (1994) 16223–16233.
[40] D. Edström, D.G. Sangiovanni, L. Hultman, V. Chirita, Thin Solid Films 571 (2014) 145–153.
[41] F. Birch, Phys. Rev. 71 (1947) 809–824.
[42] F. Birch, J. Geophys. Res. Solid Earth 83 (1978) 1257–1268.
[43] S.-L. Shang, Y. Wang, D. Kim, Z.-K. Liu, Comput. Mater. Sci. 47 (2010) 1040–1048.
[44] Y. Le Page, P. Saxe, Phys. Rev. B 65 (2002) 104104.
[45] S. Shang, Y. Wang, Z.-K. Liu, Appl. Phys. Lett. 90 (2007) 101909.
[46] G. Simmons, H. Wang, Single Crystal Elastic Stiffness Constants and Calculated Aggregate Properties: A Handbook, MIT Press, Cambridge, 1971.
[47] L. Vegard, Z. Phys. 5 (1921) 17–26.
[48] R.W.G. Wyckoff, Crystal Structures, 2nd ed. John Wiley, New York, 1963.
[49] W.B. Pearson (Ed.), International Union of Crystallography, Oosthoek, Scheltema, and Holkema, Utrecht, 1913–1993 (ZrN (Vol. 30A, p. 155), NbN (Vol. 30A, p. 155), HfN (Vol. 17, p. 70), and TaN (Vol. 35A, p. 121)).
[50] R. Heid, K.P. Bohnen, B. Renker, T. Wolf, H. Schober, Phys. Rev. B 71 (2005) 092302.
[51] J.O. Kim, J.D. Achenbach, P.B. Mirkarimi, M. Shinn, S.A. Barnett, J. Appl. Phys. 72 (1992) 1805–1811.
[52] P. Lazar, J. Redinger, R. Podloucky, Phys. Rev. B 76 (2007) 174112.
[53] C. Stampfl, W. Mannstadt, R. Asahi, A.J. Freeman, Phys. Rev. B 63 (2001) 155106.
[54] A.J. Wang, S.L. Shang, Y. Du, Y. Kong, L.J. Zhang, L. Chen, D.D. Zhao, Z.K. Liu, Comput. Mater. Sci. 48 (2010) 705–709.
[55] L. Zhou, D. Holec, P.H. Mayrhofer, J. Phys. D. Appl. Phys. 46 (2013) 365301.
[56] D.G. Sangiovanni, L. Hultman, V. Chirita, Acta Mater. 59 (2011) 2121–2134.
[57] H. Okamoto, J. Phase Equilib. 14 (1993) 336–339.
[58] S. Shang, Y. Wang, W.Y. Wang, H. Fang, Z.-K. Liu, Appl. Phys. Lett. 103 (2013) 053903.
[59] S. Shang, Y. Wang, G. Lindwall, N.R. Kelly, T.J. Anderson, Z.-K. Liu, J. Phys. Chem. C 118 (2014) 24884–24889.
[60] J.F. Nye, Physical Properties of Crystals: Their Representation by Tensors and Matrices, Oxford University Press, Oxford, 1985.
[61] X.-J. Chen, V.V. Struzhkin, Z. Wu, M. Somayazulu, J. Qian, S. Kung, A.N. Christensen, Y. Zhao, R.E. Cohen, H.-k. Mao, R.J. Hemley, Proc. Natl. Acad. Sci. U. S. A. 102 (2005) 3198–3201.
[62] W. Chen, J.Z. Jiang, J. Alloys Compd. 499 (2010) 243–254.
[63] M.B. Kanoun, S. Goumri-Said, Surf. Coat. Technol. 255 (2014) 140–145.
[64] D. Pettifor, Mater. Sci. Technol. 8 (1992) 345–349.
[65] S.F. Pugh, Philosophical Magazine Series 7, 451954. 823–843.
[66] H. Kindlund, D.G. Sangiovanni, J. Lu, J. Jensen, V. Chirita, J. Birch, I. Petrov, J.E. Greene, L. Hultman, Acta Mater. 77 (2014) 394–400.
[67] H. Kindlund, D.G. Sangiovanni, J. Lu, J. Jensen, V. Chirita, I. Petrov, J.E. Greene, L. Hultman, J. Vac. Sci. Technol. A 32 (2014) 030603.
[68] H. Kindlund, D.G. Sangiovanni, L. Martínez-de-Olcoz, J. Lu, J. Jensen, J. Birch, I. Petrov, J.E. Greene, V. Chirita, L. Hultman, APL Mater. 1 (2013) 042104.
[69] D.V. Suetin, I.R. Shein, A.L. Ivanovskii, Phys. Status Solidi B 245 (2008) 1590–1597.
[70] D.G. Sangiovanni, V. Chirita, L. Hultman, Phys. Rev. B 81 (2010) 104107.
[71] S. Appalakondaiah, G. Vaitheeswaran, S. Lebègue, N.E. Christensen, A. Svane, Phys. Rev. B 86 (2012) 035105.
[72] P. Ravindran, L. Fast, P.A. Korzhavyi, B. Johansson, J. Wills, O. Eriksson, J. Appl. Phys. 84 (1998) 4891–4904.
[73] I.N. Frantsevich, F.F. Voronov, S.A. Bokuta, in: I.N. Franstsevich (Ed.), Naukova Dumka, Kiev, 1983.
[74] M.H. Yoo, Scr. Metall. 20 (1986) 915–920.